J Mater Sci: Mater Electron (2022) 33:21762–21777

Studies on optical properties, thermal stability and electrical conductivity of copper alumina nanoparticles-reinforced Poly(pyrrole-*co*-indole) for optoelectronic devices

S. Sankar[1] and M. T. Ramesan[1,*]

[1] *Department of Chemistry, Centre for Polymer Science and Technology, University of Calicut, Calicut University P.O., Malappuram, Kerala 673 635, India*

Received: 25 April 2022
Accepted: 17 August 2022
Published online: 29 August 2022

ABSTRACT

This work focused on the effect of copper alumina (Cu–Al_2O_3) nanoparticles in poly(pyrrole-co-indole) (PPy-*co*-PIN) on optical properties, thermal stability, alternating current (AC) conductivity, direct current (DC) conductivity and dielectric properties at different temperatures. Consistent distribution of Cu–Al_2O_3 nanoparticles within the copolymer was observed from field-emission scanning electron microscopy. The single absorption seen (range 270 nm) in the UV spectra was due to π–π^* transitions in the copolymeric materials. The minimum optical bandgap energy was observed for 5 wt% nanocomposite. From thermogravimetric analysis graph, maximum thermal resistance was observed for 7 wt% nanocomposite. The AC conductivity and dielectric parameters were dependent on both temperature and nanofillers loading and the maximum properties were found for 5 wt% nanocomposite. The AC conductivity and dielectric constant of 5 wt% nanocomposites were increased by 4.5 and 3 times, respectively, in comparison to (PPy-co-PIN). The decrease in activation energy with an increase in the content of Cu–Al_2O_3 nanofillers and inverse dependence of Nyquist plot with temperature suggested semiconducting nature. The DC conductivity of copolymer was enhanced with encapsulation of Cu–Al_2O_3 -nanoparticles and the change in conductivity was correlated with Scarisbrick, Bueche and McCullough models. The McCullough model was in compromise with experimental conductivity values as it considers interfacial interactions. The match in theoretical and experimental conductivity values was advocating the presence of an efficient conductive pathway. The excellent properties of (PPy-*co*-PIN)/Cu–Al_2O_3 nanocomposites can be exploited in concocting optoelectronic devices.

Address correspondence to E-mail: mtramesan@uoc.ac.in

https://doi.org/10.1007/s10854-022-08965-5

1 Introduction

In the last few decades, the evolution observed in electronic devices is incredible. For instance, almost all new-generation devices work with wireless technology. The new and advanced technologies lead to miniaturization and also impart multi-functionality to electronic devices. However, in most cases, electronic devices experience a lower battery llifetime, thus reducing their working time. The aforementioned crisis can be curbed by the development of materials with excellent charge storage. Conducting polymers are gaining attention as charge storage devices due to their excellent dielectric properties, low cost of fabrication and high flexibility [1–4]. The conjugated double bonds within the conducting polymers can be comfortably polarized and hence exhibit high dielectric constant values. In addition to this, conducting polymers can also be used in developing devices for energy harvesting, EMI shields, gas sensing, artificial muscles and biosensing [5–8].

The frequently investigated conducting polymers are polypyrrole (PPy), polyaniline (PANI), polyindole (PIN), polythiophene (PTH) [9–12]. In the class of conducting polymers, PPy is remarkable due to the propitious polymerization of monomer, exclusive electronic properties as well as, redox characteristics and excellent environmental stability [13]. However, concocting devices from polypyrrole is a tedious task due to its limited solubility, durability and fusibility. The excellent properties of individual homopolymers are reinforced by copolymerizing pyrrole with the appropriate monomer or other conducting polymer [14]. Gherras et al. developed poly(pyrrole-*co*-2-nitrocinnamaldehyde) nanocomposites for solar cell applications [15]. Poly(biphenyl-*co*-pyrrole) synthesized by Simitzis et al. showed excellent thermal properties compared to corresponding homopolymers [16]. Wang et al. developed phytic acid-doped poly(aniline-*co*-pyrrole) for use as a supercapacitor electrode [17].

Indole is an interesting monomer to copolymerize with pyrrole since it has benzo condensed pyrrole in its structure. The copolymer developed by Köleli et al. using indole and pyrrole is shown to have excellent electrochemical properties and be suitable for a wide variety of applications [18]. In a related study, Dhanlakshmi and Saraswathi used electrochemical polymerization to make a variety of poly(pyrrole-*co*-indole) copolymers with improved electroactivity [19]. Poly(pyrrole-*co*-indole) doped with carboxylated CNT was developed by Lakourj et al. to have anticorrosion, antimicrobial, and antioxidation properties [20].

Presently, the scientific community is interested in modulating the electrical, optical and thermal properties of conducting polymers by integrating them with metal oxide nanoparticles [21–23]. The metal oxide has already proved to have exceptional properties and could be used for diverse applications [24, 25]. Metal oxide nanocomposites are used for a bunch of things, including as photocatalysis, sensors, and corrosion prevention. Conducting copolymers that have been reinforced with metal oxide nanofillers have excellent material properties. Gheymasi et al. developed nanocomposites based on poly(aniline-*co*-pyrrole) and ZnO nanoparticles with good non-linear optical properties [26]. Golsekhan et al. [27] report the existence of epoxy/(polyaniline-*co*-pyrrole)/ZnO nanocomposite coatings with excellent anti-corrosion properties.

Alumina nanoparticles are attractive among other metal oxide nanocomposites because of their mechanical and thermal properties [25]. The electrical properties of alumina nanoparticles have been reported to be enhanced by dispersion strengthening using copper ions [28]. In our previous work, an enhancement in the material properties of PIN has been observed with the reinforcement of Cu–Al_2O_3 nanofillers [29]. Thus, the hybrid composite made by the incorporation of Cu–Al_2O_3 nanofillers in the interstices of PPy-*co*-PIN could exhibit unique physicochemical traits remarkably different from the properties of polymer and nanofillers.

Conducting polymer nanocomposites are widely synthesized in a large scale by in situ chemical oxidation polymerization [30]. In comparison with electro-polymerization and ball milling techniques, the in-situ technique does not require any intricate experimental setup. Compared to the solution casting method, the in-situ technique is an environmentally benign and harmless method and can be carried out using green solvents. The homogenous administration of nanofillers over conducting polymer network via uncomplicated in-situ chemical oxidation method has already been reported in previous studies [31].

The development of optoelectronic devices requires the use of materials with good optical and

dielectric properties. In this study, we therefore synthesized novel (PPy-*co*-PIN)/Cu–Al_2O_3 nanocomposites and investigated their optical characteristics, thermal stability, morphology, and temperature-dependent dielectric parameters. The increase in DC conductivity of copolymer with the addition of Cu–Al_2O_3 nanoparticles was also correlated with different theoretical models based on Scarisbrick, Bueche and McCullough in order to study the mechanism of conduction in copolymer hybrids.

2 Experimental details and characterizations

2.1 Materials and methods

The indole, pyrrole, oxidant ($FeCl_3$), sodium dodecyl sulphate (SDS), copper nitrate (Cu $(NO_3)_2$), aluminium nitrate (Al $(NO_3)_3$), urea, HCl and methanol required for the in-situ method were of analytical grade from Merck India. The synthesis procedure was carried out in double-distilled water.

2.2 Synthesis of Cu–Al_2O_3 nanopowder

The thermo-chemical mode was employed for the synthesis of copper alumina nanoparticles [27]. The aqueous solutions of urea, Cu $(NO_3)_2$ and Al $(NO_3)_3$ were mixed in 1:2:3 ratios. The aqueous solution was kept at 100 °C till a hydrogel was obtained. The hydrogel obtained was finally combusted in a muffle furnace at 500 °C.

2.3 Synthesis of poly (pyrrole-*co*-indole) copolymer

The pyrrole and indole were copolymerized via oxidation using ferric chloride as an oxidant. In a three-neck flask, 1.0 M $FeCl_3$ was made by dissolving in an appropriate quantity of water. To the oxidant solution, the acidic aqueous solution containing an equimolar (0.5 M) quantity of pyrrole and indole was slowly added using a dropping funnel. The mixture was constantly stirred and within a few minutes, the colour of the solution was converted from red to dark green. This colour change indicated the copolymerization of pyrrole and indole. After consistent stirring for 8 h, the copolymer obtained was washed with water and methanol to remove the left-over monomers and oxidant. Finally, the copolymer was dried in a vacuum oven at 60 °C for 24 h.

2.4 Synthesis of poly(pyrrole-*co*-indole)/ Cu–Al_2O_3 nanocomposites

The (PPy-*co*-PIN)/Cu–Al_2O_3 nanocomposites were successfully synthesised by in-situ chemical oxidation polymerization. Copper alumina nanoparticles (3, 5 and 7 wt%) were mixed with SDS in distilled water. The dispersed nano-solutions were added to the pyrrole/indole (1:1 ratio) with constant stirring and ultrasonicated for 30 min. The FeCl3 solution (1 M) was then added dropwise to the homogeneous solution of monomers and the copolymerization was continued for a period of 8 h at room temperature. Finally, the greenish-black precipitate formed was filtered, washed and dried in a vacuum oven.

2.5 Instrumentation

The UV spectrum of (PPy-*co*-PIN)/ Cu–Al_2O_3 nanocomposites were recorded using a JASCO V-770 spectrophotometer. The FESEM images of (PPy-*co*-PIN)/Cu–Al_2O_3 nanocomposite were obtained using the Carl Zeiss VP-500 model. The thermal resistance of the (PPy-*co*-PIN)/ Cu–Al_2O_3 nanocomposites was recorded in Hitachi STA7200 thermogravimetric analyser and the sample was heated from 25 to 600 °C at a heating rate of 10 °C/min. The AC electrical properties, dielectric parameters and DC conductivity of samples (pelletized using a hydraulic press) at various temperatures were measured in the range of 10^2 to 10^6 Hz using a Hioki 3570 Model.

3 Results and discussion

3.1 Field emission scanning electron microscopy (FE-SEM)

FE-SEM images of PPy-*co*-PIN and (PPy-*co*-PIN)/Cu–Al_2O_3 nanocomposites at 200 nm magnification are given in Fig. 1. The SEM image of PPy-*co*-PIN exhibits cragged morphology. Considerable change in the morphology of PPy-*co*-PIN is observed with reinforcement of nanofillers. Cu–Al_2O_3 nanofillers in polyindole with spherical shapes have previously been described in our earlier study [29]. The spherical

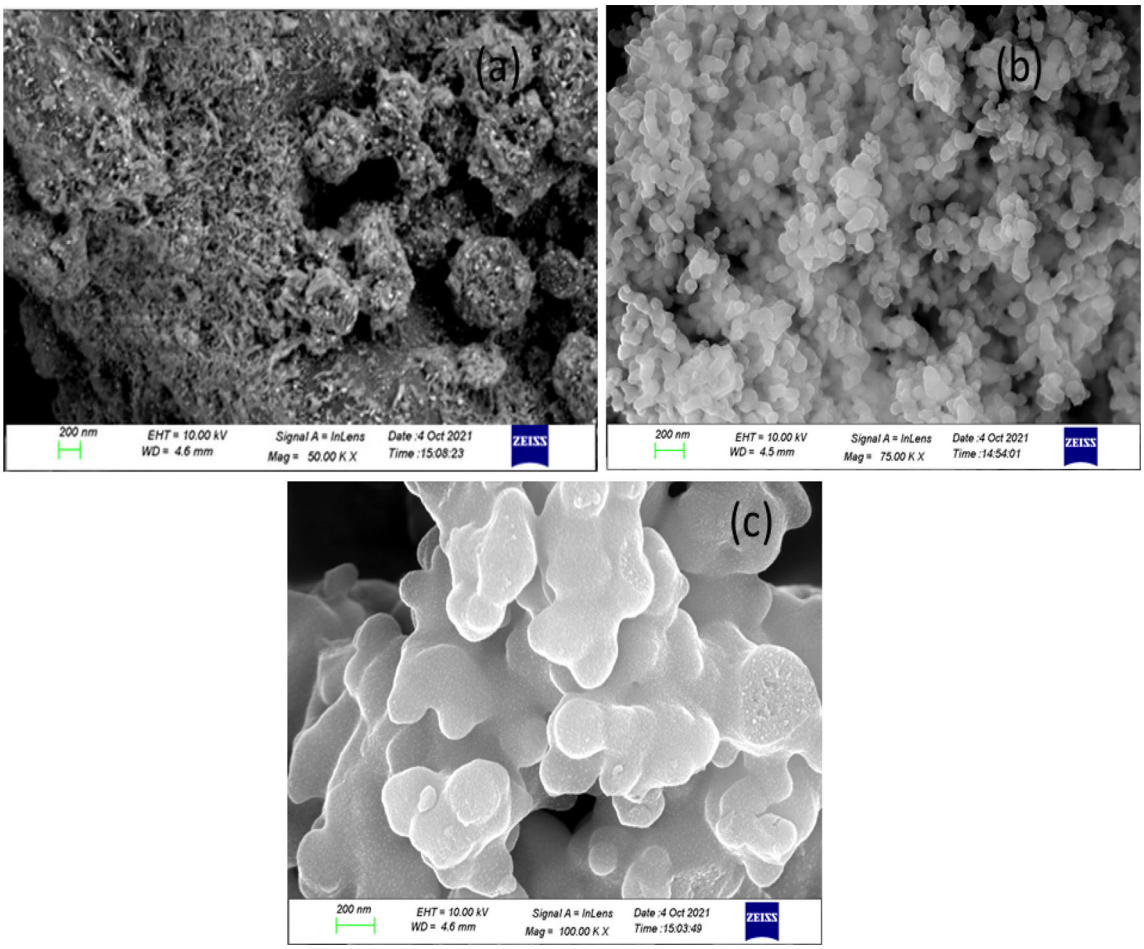

Fig. 1 FE-SEM images of **a** PPy-*co*-PIN, **b** 5 wt% and **c** 7 wt% Cu–Al_2O_3 at 200 nm magnification

morphology of nanocomposites arises from the interaction of polar groups of copolymers with nanomaterials. The composite with a 5 wt% sample shows a better distribution of nanomaterial. The uniform adhesion between the copolymer and nanomaterial is the cause of this homogenous dispersion. Here, the nanoparticles in the composites are found to be agglomerated at higher loading (7 wt%). The short interparticle distance in higher loading causes a diminishing interfacial interaction. SEM images clearly demonstrate the successful formation of (PPy-*co*-PIN)/ Cu–Al_2O_3 nanocomposites.

3.2 UV–Visible spectroscopy

Figure 2 shows the electronic absorption spectra of PPy-*co*-PIN and (PPy-*co*-PIN)/Cu–Al_2O_3 nanocomposites. For PPy-*co*-PIN, a single absorption at 275 nm is observed. This absorption band is the resultant of π to π^* transitions existing in the

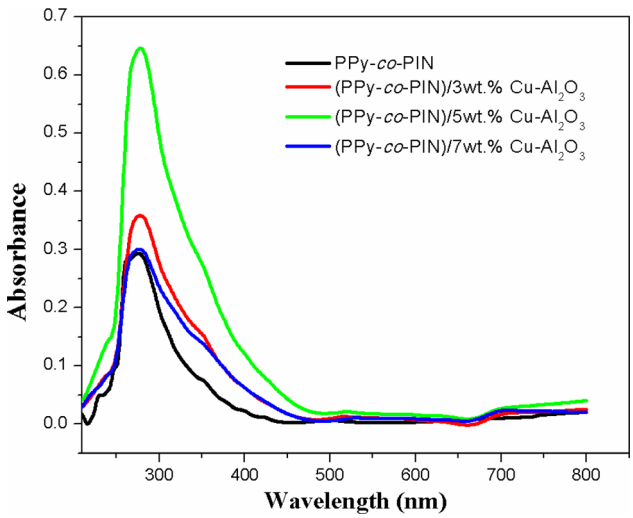

Fig. 2 UV spectrum of PPy-*co*-PIN and its nanocomposites

copolymer. The presence of this band suggests the existence of charge transfer through the conjugated

structure comprising of indole and pyrrole monomer units.

Comparing the UV spectrum of the (PPy-*co*-PIN)/Cu–Al_2O_3 nanocomposites and pure copolymer, the former is found to have larger values for absorption intensity. Further, a redshift in absorption maximum is also observed. The altering of electronic structure aided by robust interaction between nanofillers and copolymer is the reason for the aforementioned observations. The magnitude of the absorption maximum of (PPy-*co*-PIN)/Cu–Al_2O_3 nanocomposites follows the order 5 wt% > 3 wt% > 7 wt% loading. The maximum absorption in 5 wt% composite arises from the effective dissemination of Cu–Al_2O_3 nanofiller. The decrease in absorption in 7 wt% can be assigned to the aggregation of Cu–Al_2O_3 nanofillers in the nanocomposites.

Figure 3 shows the UV–Vis transmittance spectrum of PPy-*co*-PIN and Cu–Al_2O_3 wrapped copolymer nanocomposites. The entire sample exhibits excellent transmittance in the region of visible light. The predominant UV shielding capability of synthesized samples is perceived from the fall in transmittance in UV wavelength region [32]. Moreover, the UV screening capacity of (PPy-*co*-PIN)/Cu–Al_2O_3 nanocomposites is higher than that of pristine copolymer. The UV light falling on the nanocomposites is well absorbed and scattered by the Cu–Al_2O_3 nanofillers encapsulated within the copolymer. Among the materials, 5 wt% nanocomposite shows excellent UV shielding characteristics due to the efficient distribution of metal oxide nanofillers. The

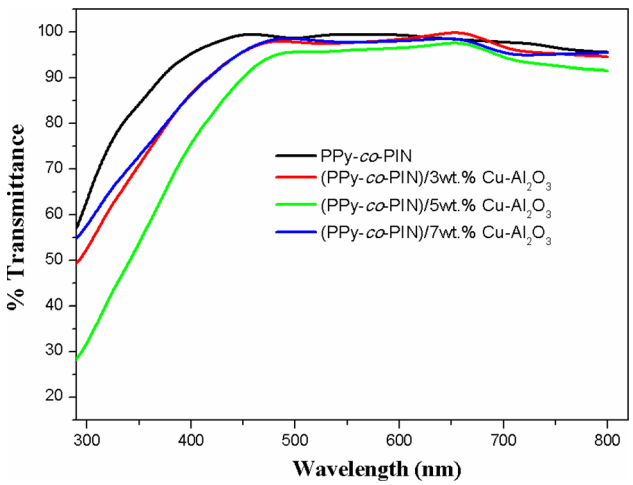

Fig. 3 UV transmittance spectrum of copolymer and copolymer/Cu–Al_2O_3 nanocomposites

lower UV resistance is observed for 7 wt%, aggregation of Cu–Al_2O_3 nanofillers within the polymer matrix, which is the least effective in absorbing and scattering UV radiations.

3.2.1 *Optical bandgap energy*

The awareness of optical bandgap energy is vital in investigating the optoelectronic applications of the materials. The filled valence band and vacant conduction band in polymeric materials are separated by a small distance and the minimum energy essential for the electronic excitation from the former to the latter is referred to as the optical bandgap. The photoexcitation occurring in copolymers follows the Tauc relation [33].

$$(\alpha h\upsilon)^n = \beta\left(h\upsilon - E_g\right), \quad (1)$$

(α) in the above equation is related to an absorption coefficient (α = absorbance/path length), B represents the probability transition constant, hν corresponds to photon excitation energy, E_g refers to bandgap energy and the value of n governs the nature of transition ($n = 2$ for direct transitions and $n = ½$ for indirect transitions). The Tauc plots of both direct and indirect transitions of the copolymer and its nanocomposites are presented in Fig. 4. As the content of Cu–Al_2O_3 increases in the copolymer, bandgap energies decrease due to the Lewis acid nature of Cu–Al_2O_3 that can accept an electron from heteroatoms in the copolymeric system. The lowest bandgap energy for 5 wt% nanocomposite can be attributed to the charge transfer facilitated by the constant distribution of Cu–Al_2O_3 nanofillers. The increased bandgap of the 7 wt% sample indicates the development of some structural irregularities within the system.

3.3 Thermogravimetric analysis (TGA)

The TGA graph of PPy-*co*-PIN with different contents of Cu–Al_2O_3 is given in Fig. 5. The nature of the TGA profile of pristine PPy-*co*-PIN reveals a two-step degradation. The first degradation observed between room temperature and 97 °C corresponds to the eviction of water molecules enmeshed within the copolymer nanocomposites and also to the dislodging of dopant ions and unreacted monomers from the material. The second stage of weight loss from 207 to 471 °C arises from the degradation of the copolymer

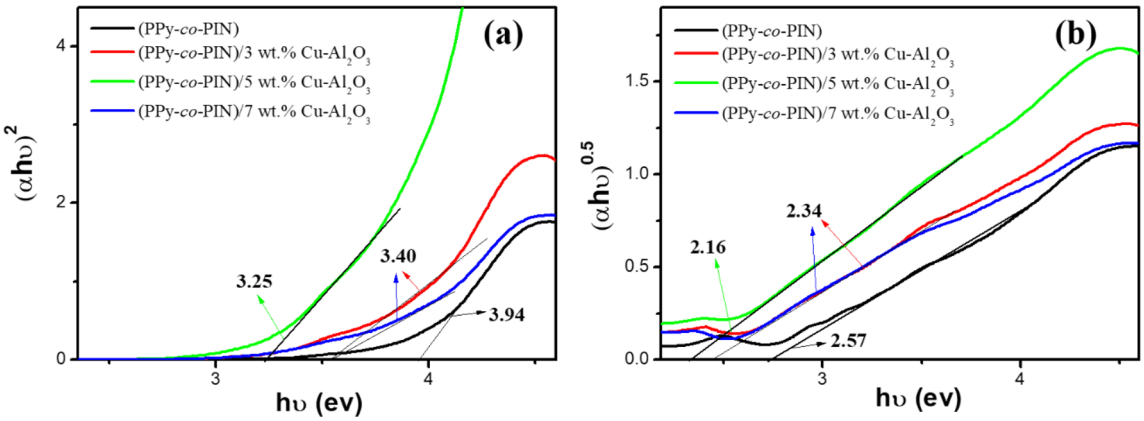

Fig. 4 The direct and indirect bandgap energy of copolymer and its nanocomposites using Tauc plot

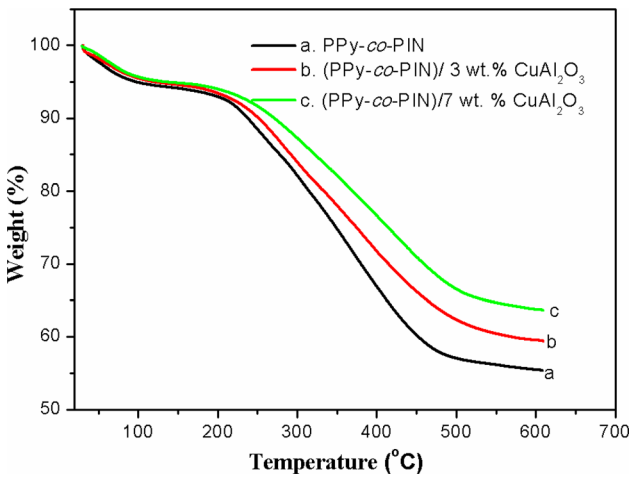

Fig. 5 TGA of PPy-*co*-PIN and (PPy-*co*-PIN)/Cu–Al_2O_3 nanocomposites

matrix. In comparison with our earlier studies, the copolymer has better thermal stability than polypyrrole (169 °C) [34]. The improved thermal stability of copolymer suggests a higher degree of crosslinking between homopolymers [35].

The copolymer decomposition in 5 and 7 wt% nanocomposites start at 223 and 235 °C, respectively, suggesting the strong dependence of thermal stability on the reinforced Cu–Al_2O_3 nanoparticles. These results point towards the growth of a copolymeric phase within the Cu–Al_2O_3 nanofillers (confirmed by FE-SEM results) and the barrier effect of metal oxide nanofillers. The barrier effect and interfacial interaction hinder both segmental motion and chain transfer reactions of the copolymer [36]. Similarly, carbonaceous contents at 600 °C existing in PPy-*co*-PIN is found to be 55.5%, increased to 59.6% in 3 wt% loading and 63.7% in 7 wt% loading nanocomposites. The higher carbonaceous contents suggest the excellent flame resistance of (PPy-*co*-PIN)/Cu–Al_2O_3 nanocomposites.

3.4 Dielectric constant

Analysis of the dielectric constant of PPy-*co*-PIN and (PPy-*co*-PIN)/Cu–Al_2O_3 nanocomposites with frequency at various temperatures (Fig. 6) gives us an idea about their capacitive and conductive identity. The capacitive identity of the copolymer gives an idea about amount of electrical charge that can be stored within the material. The conductive identity denotes charge transfer occurring within the material. When exposed to an alternating electric field, the dielectric constant varies with frequency. The inverse relation of the dielectric constant with frequency is the result of various polarization processes occurring in the material [37]. The maximum values of dielectric constant at lower frequencies can be ascribed to dipolar polarization. The lining up of perpetual dipoles in the copolymeric system at lower frequencies leads to dipolar polarization. While the lining up of permanent dipoles with the field is tedious at higher frequencies. This is due to the rapid fluctuation of the alternating field. Thus, the dipolar vibrations lag behind the applied electric field, resulting in minimum polarization and dielectric constant values. This enhancement in dielectric constant can be attributed to the significant segmental motion of dipoles within the copolymeric system at high temperatures [38]. The absorbed thermal energy in the polymeric material reduces the energy barrier for the reconstitution of dipoles [39].

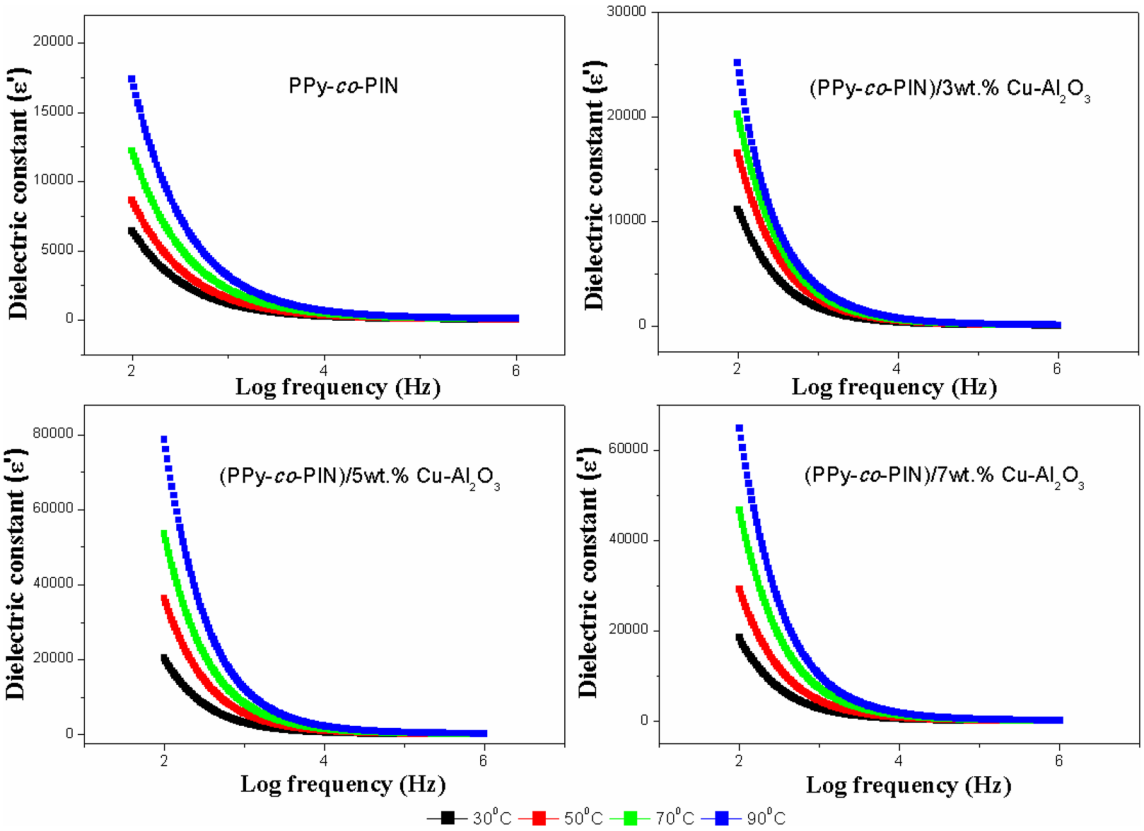

Fig. 6 Dielectric constant of copolymer and its nanocomposites at different temperatures

The magnitude of dielectric constant is intensified with the increase in the content of Cu–Al_2O_3. For instance, the magnitude of dielectric constant of (PPy-*co*-PIN)/5 wt% Cu–Al_2O_3 nanocomposite at room temperature (ε' = 20,417) is 3 times higher than bare copolymer (ε' = 6422) and 1.8 times intensified when compared with 3 wt% nanocomposite (ε' = 11,169). This points out that the incorporation of Cu–Al_2O_3 nanofillers enhances the interfacial polarization within the material and generates a conductive network within the organic–inorganic hybrid [40]. However, the dielectric constant value of 7 wt% nanocomposites is lower than that of 5 wt% nanocomposite. The better morphology of (PPy-*co*-PIN)/5 wt% Cu–Al_2O_3 nanocomposite allows the swift oscillation of dipoles thus resulting in maximum dielectric constant values. The aggregation of Cu–Al_2O_3 nanofillers in (PPy-*co*-PIN)/7 wt% Cu–Al_2O_3 nanocomposite restricts the segmental mobility of dipoles, hence experiencing lower dielectric constant values. The higher dielectric constant of copolymer nanocomposites can be utilized in designing various semiconductor devices [39]. (PPy-*co*-PIN)/Cu–Al_2O_3 nanocomposites have a higher dielectric constant than the nanocomposites comprised of a poly(pyrrole-*co*-aniline) matrix and ZnO nanoparticles [41].

3.5 Dielectric loss

The variation of dielectric loss with frequency (Fig. 7) gives us an insight into energy disintegration occurring in the PPy-*co*-PIN and their nanocomposites with Cu–Al_2O_3 in an applied electric field. The maximum value of dielectric loss is observed at 100 Hz for entire samples. The maximum energy dispersion indicates the existence of insulating grain boundaries. Thus, extra energy is necessary for the hopping of charges. The energy dissipation is reduced by boosting the frequency values. Once it reaches a certain frequency, the energy dissipation becomes frequency independent due to the weak polarization of the system. The dielectric property increases with temperature due to enhanced charge carrier movements. The higher value of the dielectric loss at 100 Hz and 90 °C can be attributed to the

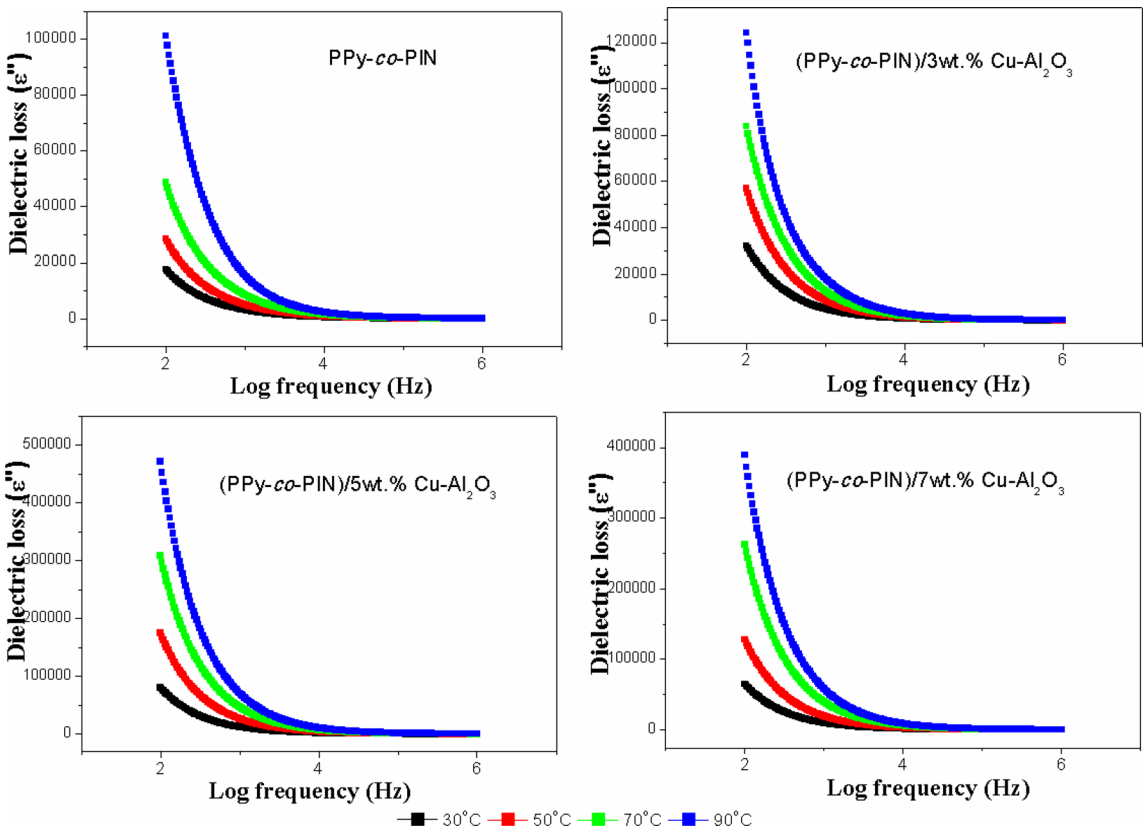

Fig. 7 Dielectric loss of copolymer and its nanocomposites at different temperatures

aggregation of charges at grain partitions. Further, it is observed that the ε'' values at lower frequencies are intensified with an increase in filler content. The reinforcement of nanofillers enhances the movement of dipoles, which contributes to energy dissipation. The maximum value for dielectric loss at 100 Hz is observed for 5 wt% loading. The efficient dispersion of nanofillers in this loading maximizes the mobility of bound charges. The clustering of Cu–Al_2O_3 nanofillers at 7 wt% restricts the dipolar motion and thus experiences minimum energy dissipation.

3.6 Alternating current (AC) conductivity

The variation of AC conductivity (σ_{ac}) of PPy-*co*-PIN and its nanocomposites at different temperatures is illustrated in Fig. 8. The graph suggests that the AC conductivity of all samples is proportional to the applied frequency. This dependency points towards the highly compactable copolymer network formed between indole and pyrrole monomers. The AC conductance arises from the motion of charges in the disordered copolymeric system when exposed to an electric field [42]. The high temperatures enable unbounding of charge carriers that could easily tunnel through the frequency barricade, hence enhancing the conductivity [43]. The AC conductivity values of PPy-*co*-PIN are enhanced with the addition of Cu–Al_2O_3 nanofillers. The variation of AC conductivity with the content of Cu–Al_2O_3 nanofillers at 100 Hz and different temperatures is given in Fig. 9. The interfacial interaction between Cu–Al_2O_3 nanofiller and the copolymer reduces the inter-chain distance and creates new electrical states, thereby creating a new conduction path [44].

The maximum AC conductivity for (PPy-*co*-PIN)/5wt% Cu–Al_2O_3 nanofillers arises from the efficient distribution of nanofillers. The efficient distribution of nanofillers aids the formation of interconnected conductive networks of Cu–Al_2O_3 nanofillers within the pristine PPy-*co*-PIN. The decrease in AC conductivity in (PPy-*co*-PIN)/7wt% Cu–Al_2O_3 nanocomposites can be attributed to the depletion of the localized sites due to aggregation of Cu–Al_2O_3 nanofillers. The higher AC conductivity value of the 5 wt% nanocomposite suggests that the material is appropriate for use in the semiconductor industry.

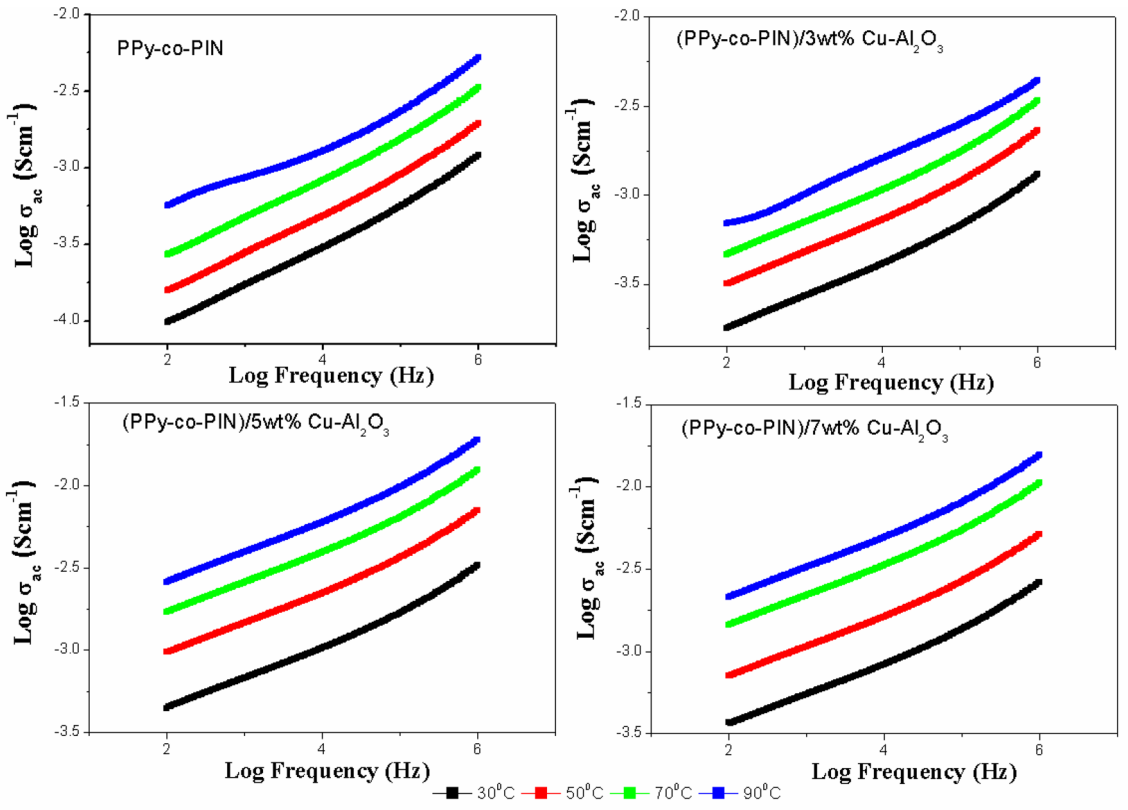

Fig. 8 AC conductivity of copolymer and its nanocomposites at different temperatures

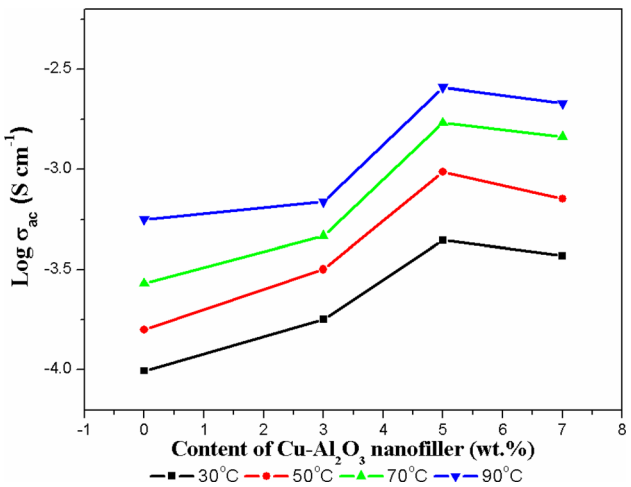

Fig. 9 The variation of AC conductivity with content of Cu–Al_2O_3 nanofillers at 100 Hz

3.6.1 *Activation energy*

The temperature dependency of AC conductivity can be mathematically represented as

$$\sigma_{ac} = \sigma_0 \exp\left(\frac{-E_a}{KT}\right). \quad (2)$$

here in this relation E_a, K, T and σ_0 refer to the activation energy, Boltzmann constant, absolute temperature and pre-exponential factor, respectively. The σ_{ac} Vs 1000/T plot is shown in Fig. 10. It gives us the activation energy of samples. The values of the activation energy of all samples are provided in Table 1. In the nanocomposites, a conductive network promotes large-scale hopping of charge carriers, eventually reducing the activation energy.

3.7 Electric modulus and Nyquist plot

The electric modulus of a material can be explained as the multiplicative inverse of the dielectric constant. The real part of the electric modulus gives us insights into charge storage while the imaginary part is associated with energy loss. The plot of M' vs frequency of entire samples at different temperatures is shown in Fig. 11. The trivial values of M' and frequency independence of all samples in the initial frequency ranges indicate the conduction arising from the movement of loosely bound charges. Moreover, this observation also cancels out the

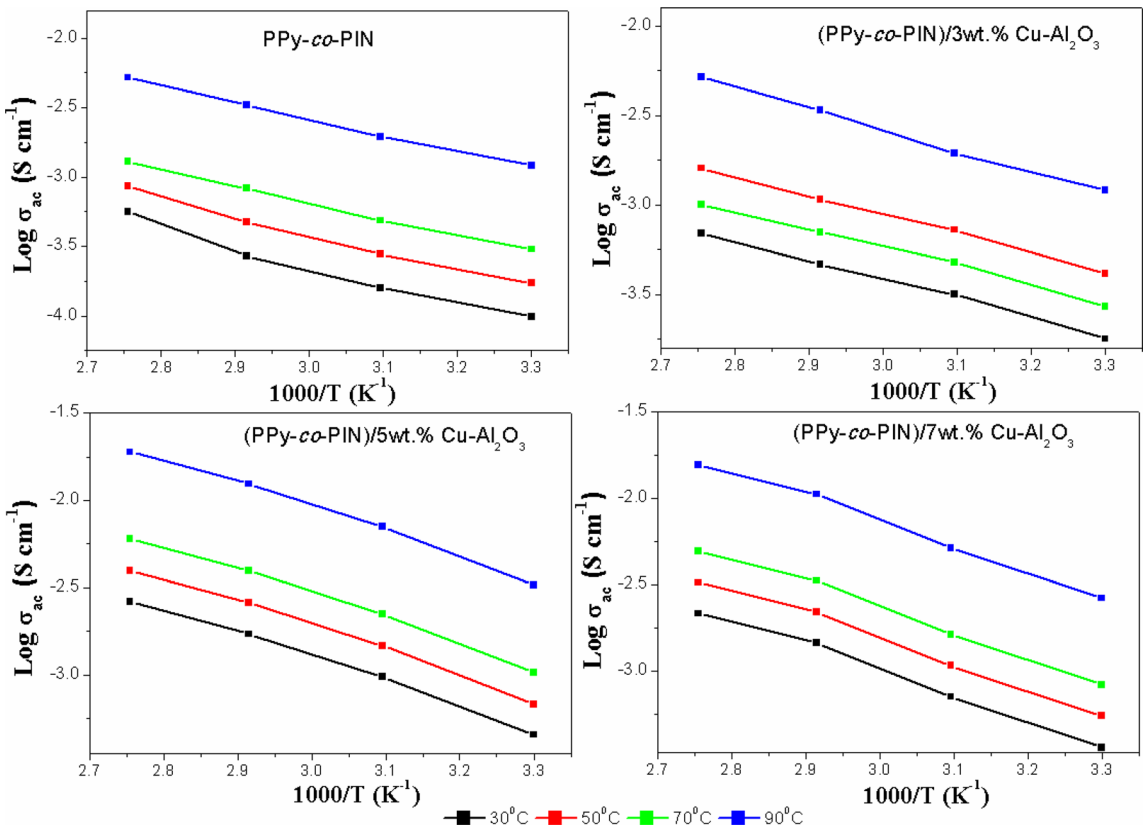

Fig. 10 The log σ_{ac} Vs 1000/T plot of PPy-*co*-PIN and its nanocomposites

Table 1 Variation of E_a with content of Cu–Al_2O_3 nanofiller at 1 MHz

Copolymer/loading of Cu–Al_2O_3 (%)	Activation energy (eV) at 1 MHz
0	1.97
3	1.53
5	1.14
7	1.43

possibility of electrode polarization. The larger value of M' is observed at higher frequencies, which can be attributed to conduction arising from the tentative oscillation of charge carriers associated with rapidly switching of polarity at high frequencies and a minimum reinstating force that initiates the movement of ions [45].

The plot of M'' *Vs* log F illustrated in Fig. 12 shows almost identical behavior to M' *Vs* log frequency plot. The frequency independence at lower frequencies manifests the effortless hopping of charge carriers. While at higher frequencies, only bound charges are dominant and those can only move in immediate vicinities. The absence of dips at higher frequencies implies a brief relaxation time. Moreover, with an increase in temperature M'' values of all samples are shifted to higher frequencies. This inference indicates the tunneling of charge carriers at high temperatures [46].

It is evident that the magnitude of M' and M″ of PPy-*co*-PIN is decreased with the reinforcement of Cu–Al_2O_3 nanofillers. This suggests the presence of short-range motions of charge carriers originated during composite formation. The minimum values of M' and M″ are observed for (PPy-*co*-PIN)/5 wt% nanocomposite, suggesting an efficient interfacial interaction. The excellent interfacial interaction generates an alley for efficient hopping of charges. The interaction diminishes with further loading of nanofiller as explained in SEM results, thus observing an increase in value of M' and M″ for higher loading (7 wt%) when compared with 5 wt% nanocomposite.

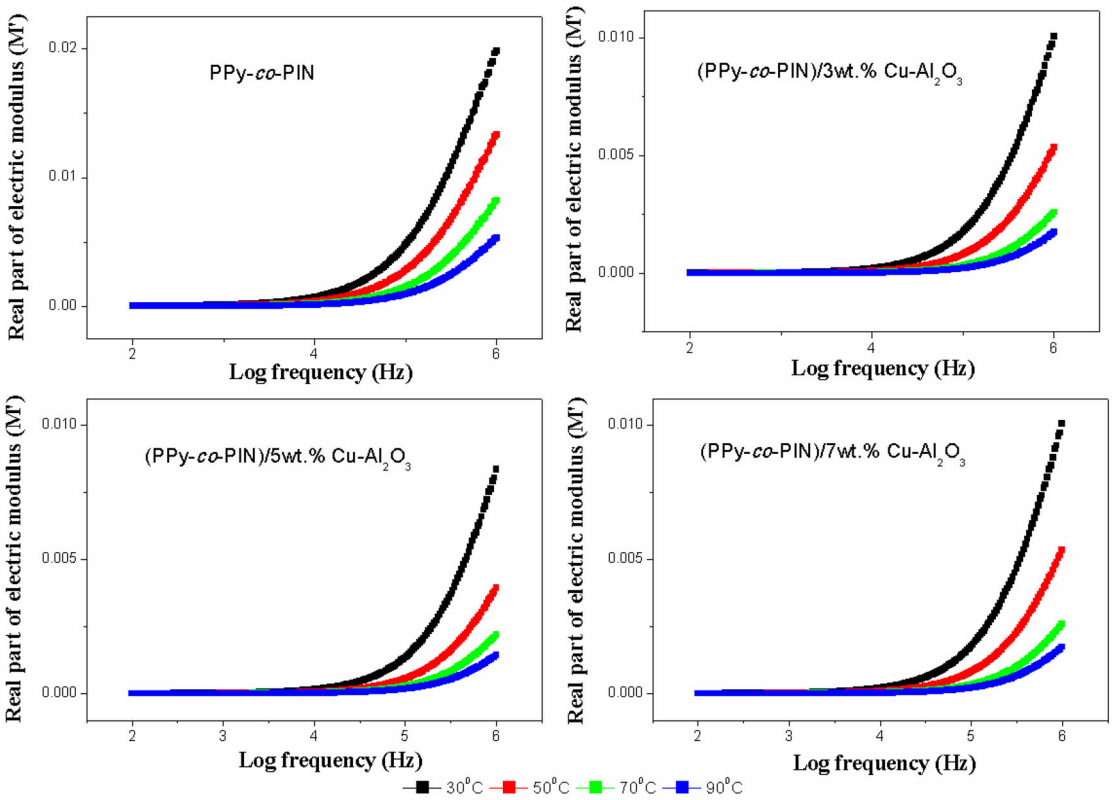

Fig. 11 M′ Vs log frequency of PPy-*co*-PIN and its nanocomposites

Figure 13 indicates the Nyquist plot (*M′ Vs M″*) of PPy-*co*-PIN and (PPy-*co*-PIN)/Cu–Al_2O_3 5 wt% nanocomposites at different temperatures. The single arc centering at the origin in the Nyquist plot manifests a single relaxation process occurring in the material [47]. This relaxation process corresponds to the bulk resistance of the copolymer. The arc diameter of the (PPy-*co*-PIN)/Cu–Al_2O_3 5 wt% nanocomposite is less when compared with that of the pristine copolymer. The reduction of arc diameter manifests increments in conductivity. Similarly, a reduction in arc width is observed when the temperature is increased. The inverse relationship existing between resistance and temperature indicates the semiconducting nature of the materials. The Nyquist plot validates the results obtained from other dielectric studies performed.

3.8 Direct current (DC) conductivity

The DC conductivity of (PPy-*co*-PIN)/Cu–Al_2O_3 nanocomposites at different compositions is shown in Fig. 14. The (PPy-*co*-PIN)/Cu–Al_2O_3 nanocomposites showed an enhanced conductivity than PPy-*co*-PIN. This enhancement arises from the long-range order of copolymeric fragments imparted by Cu–Al_2O_3 as well as the robust alliance that originating between interfaces. A significant change in DC conductivity is observed in varying the composition of nanofillers. A notable enhancement in conductivity is observed in increasing the composition of Cu–Al_2O_3 nanoparticles. While only a little enhancement is observed on increasing the composition of Cu–Al_2O_3 nanofillers beyond 5 wt%. This points to the better association between the organic and inorganic phases in the 5 wt% composite.

3.9 Scarisbrick model

The theoretical Scarisbrick model evaluates the contribution of inter-particle contact in generating conductive networks within the hybrid copolymer nanocomposites [48]. According to this model, the conductivity of conducting copolymer nanocomposites can be represented as follows:

$$\frac{\sigma_c}{\sigma_f} = C^2 \Psi \Psi \left[\exp\left(\Psi^{-\frac{2}{3}} \right) \right], \tag{3}$$

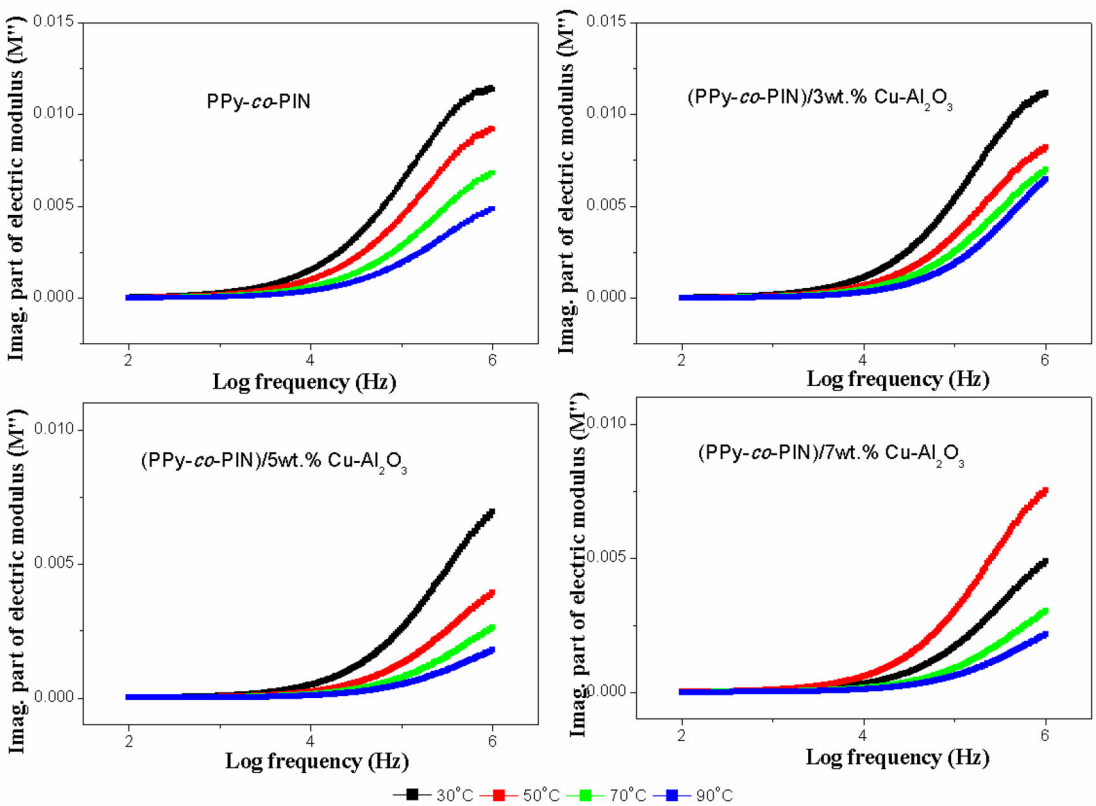

Fig. 12 M″ Vs Log f plot of PPy-*co*-PIN and (PPy-*co*-PIN)/Cu–Al2O3 nanocomposites

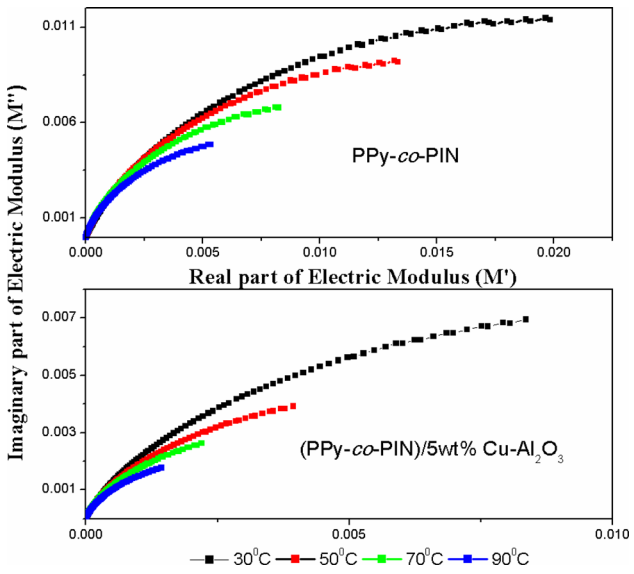

Fig. 13 Nyquist plot of copolymer and copolymer/5 wt% Cu–Al_2O_3 nanocomposite

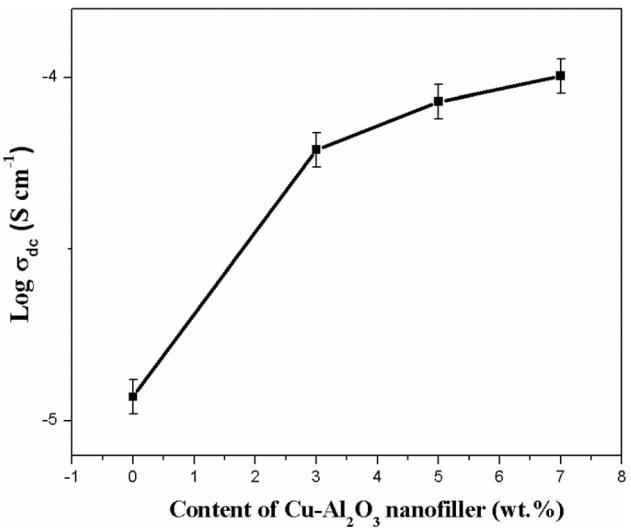

Fig. 14 Variation of DC conductivity of copolymer with Cu–Al_2O_3 loading

where σ_c, σ_f, ψ and C are the conductivity of the composite, conductivity of nanofillers, volume fraction of nanofillers in the hybrid and the geometrical factor, respectively. The values of the geometrical factor (C^2) range between 1 and 3×10^{-3}. The comparison of conductivity obtained from Scarisbrick model and experimental conductivity is presented in Fig. 15. The theoretically obtained conductivity is higher in magnitude than the experimentally

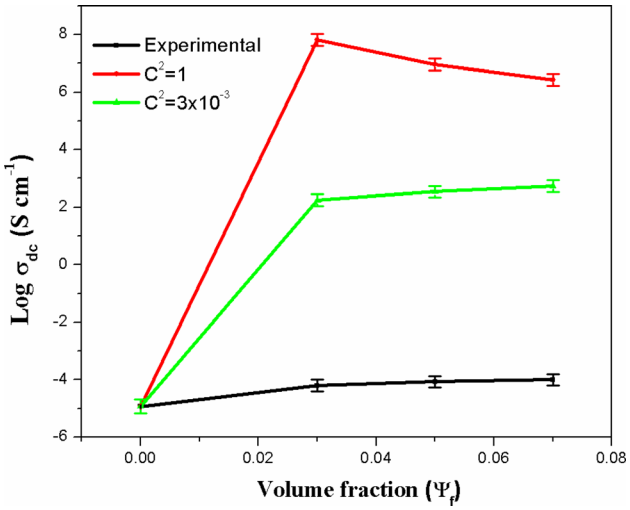

Fig. 15 Comparison of experimental conductivity with Scarisbrick theoretical model

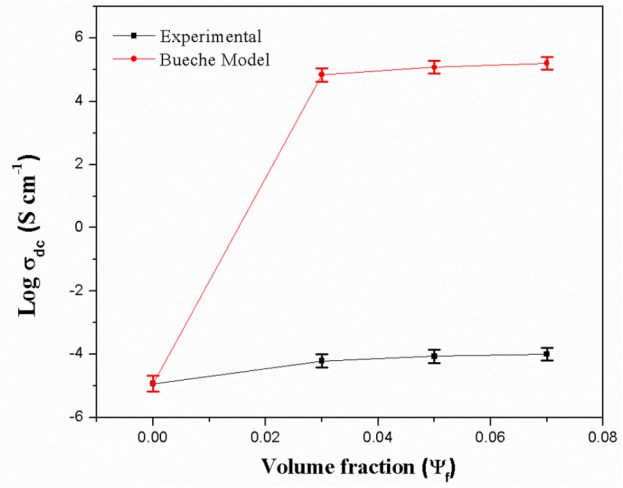

Fig. 16 Comparison of experimental conductivity with Bueche theoretical model

obtained conductivity. This huge variation in conductivity calculated from Scarisbrick model can be attributed to the disregarded contribution of the copolymer matrix towards conductivity. Moreover, it is tedious to measure the actual values of geometrical factors (C^2) and which also contributes to the aforementioned variations.

3.9.1 *Bueche model*

The Bueche model suggested an equation to calculate the conductivity of a heterogeneous hybrid system made by reinforcing conducting nanofillers within the copolymer backbone [49]. The Bueche equation can be represented as

$$\sigma_c = \sigma_f \Psi_f + \sigma_p (1 - \Psi_f), \tag{4}$$

where σ_f, σ_p, represent the conductivity parts (conductivity of filler and conductivity of copolymer respectively). The Ψ_f in the Bueche equation corresponds to volume fraction. Thus, Bueche model considers the contribution of both filler particles and copolymer toward conductivity.

According to this model, the accumulation of nanofillers in the system and interfacial interaction generate a conductive path within the copolymeric abutment. The plot given in Fig. 16 represents the plot that compares the experimentally measured conductivity and theoretical conductivity values (Bueche model) of the copolymer. The plot suggests that the conductivity values at lower content of Cu–Al_2O_3 nanofillers formulated from Bueche model is far distinct from those measured experimentally. The failure of Bueche model in (PPy-co-PIN)/Cu–Al_2O_3 nanocomposite system suggests the variable conductivity of copolymer and nanofillers.

3.9.2 *McCullough model*

The conductivity model suggested by McCullough is helpful in determining the DC conductivity of copolymer nanocomposites. This model accounts for the DC conductivity emanating from the transport behaviour in inorganic/copolymer hybrid nanocomposites [50]. The transport properties of material are a function of the amount of filler content and the conductive network formed between the interfaces. The conductivity of copolymer nanocomposites using this model can be expressed as

$$\sigma_c = \sigma_p \Psi_p + \sigma_f \Psi_f - \left[\frac{\lambda \Psi_p \Psi_f (\sigma_f - \sigma_p)^2}{V_f \sigma_f + V_p \sigma_p} \right], \tag{5}$$

σ_f, σ_p, Ψ_f, Ψ_p and λ in this equation pertain to the conductivity of filler, conductivity of copolymer, the volume fraction of nanofillers, the volume fraction of the copolymer and structural factor respectively. The values of structural factors vary between 0 and 1. Using the following equations, the V_f and V_p values can be determined.

$$V_f = (1 - \lambda)\Psi_f + \Psi_p \lambda, \tag{6}$$

$$V_p = (1 - \lambda)\Psi_p + \Psi_f \lambda. \tag{7}$$

Theoretical DC conductivity is measured by the aforementioned equation using λ = 0, 0.5, 0.9 and 1. Both the theoretical and experimental conductivity values are compared in Fig. 17. It is obvious that theoretical conductivity corresponding to λ = 1 has similar nature and values with the experimentally obtained electrical conductivity. The identical theoretical and experimental values of conductivity suggest the excellent transport behaviour resulting from the generation of an efficient conductive pathway.

4 Conclusions

We have developed copper alumina nanoparticles embedded poly(pyrrole-co-indole) with high dielectric constant, dielectric loss, conductivity, impedance, optical property and thermal stability using varying weight percentages of (3, 5, 7 wt%) Cu–Al_2O_3 dispersed in (PPy-*co*-PIN). The FESEM image of 5 wt% nanocomposite confirmed the uniform dispersion of Cu–Al_2O_3 nanofillers in the copolymer. The UV absorption studies show large absorption maximum and minimum bandgap energy for (PPy-*co*-PIN)/5 wt% Cu–Al_2O_3 nanocomposite suggesting better interfacial interaction with the copolymer. The UV transmittance spectrum of copolymer nanocomposites indicated their UV screening nature. The nanoparticles in the copolymer inhibit thermal degradation and the thermal stability increases with the loading of Cu–Al_2O_3. The higher thermal stability of copolymer nanocomposites was due to the barrier effect of Cu–Al_2O_3 nanofillers and interfacial interaction between inorganic and organic phase. The dielectric constant of PPy-*co*-PIN at room temperature was measured to be 6422, and it increased to 11,215, 20,417, and 18,607 for Cu–Al_2O_3 nanocomposites at 3 wt%, 5 wt% and 7 wt% samples. The increase in dielectric properties related to the reinforcement of Cu–Al_2O_3 nanofillers may be the result of higher ordering in nanocomposites. The addition of Cu–Al_2O_3 nanofillers reduced the inter-chain spacing and increased the AC conductivity. With the incorporation of Cu–Al_2O_3 nanofillers, the inter-chain distance was reduced and hence experiences excellent AC conductivity. The AC conductivity of PPy-*co*-PIN, 3, 5 and 7 wt% nanocomposites was determined to be − 3.25, − 3.12, − 2.59 and − 2.67 cm^{-1} respectively, at 90 °C. The highest AC conductivity and dielectric properties reported for the nanocomposite with a 5 wt% was due to the homogenous dispersion of Cu–Al_2O_3 nanofillers in the PPy-*co*-PIN matrix. The studies on the real and imaginary part of the electric modulus indicated brief relaxation times of synthesized materials. The decrease in diameter of the arc in Nyquist plot with reinforcement of Cu–Al_2O_3 nanofillers confirmed the decrease in bulk resistance. The DC conductivity was improved with the content of Cu–Al_2O_3 nanofillers and the experimental DC conductivity agrees well with the McCullough theoretical model. The remarkable optical, thermal, electric, and dielectric properties of the materials may be effectively utilised in the design of opto-electronic devices for sensing and charge storage.

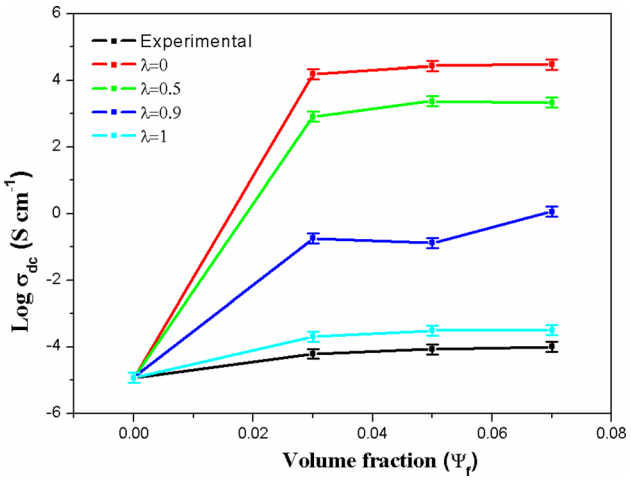

Fig. 17 Comparison of experimental conductivity with McCullough theoretical model

Author contributions

All authors contributed to study conception and design. SS contributed to the writing, analysis, and methodology, while MTR contributed on the conception, resources, validation, and writing, review and editing.

Funding

There is no funding available for the research.

Declarations

Conflict of interest The authors declare no competing interests.

Ethical approval The research doesn't involve studies with animals and human.

Consent of publication The authors have read the content and approved for submission of this manuscript to Journal of Materials Science: Materials in Electronics.

Data availability All data generated or analysed during this study are available with the authors.

References

1. G. Sowmiya, G. Velraj, J. Mater. Sci. Mater. Electron. **31**, 14287 (2020)
2. S. Shenbagavalli, M. Muthuvinayagam, S. Jayanthi, S. Revathy, J. Mater. Sci. Mater. Electron. **32**, 9998 (2021)
3. H. Derakhshankhah, R. Mohammad-Rezaei, B. Massoumi, M. Abbasian, A. Rezaei, H. Samadian, M. Jaymand, J. Mater. Sci. Mater. Electron. **31**, 10947 (2020)
4. L. Zou, X. Duan, W. Zhou, H. Zhang, S. Chen, J. Chai, X. Liu, L. Shen, J. Xu, G. Zhang, J. Mater. Sci. Mater. Electron. **30**, 7850 (2019)
5. N. Sorkhishams, B. Massoumi, M. Saraei, S. Agbolaghi, J. Mater. Sci. Mater. Electron. **30**, 21117 (2019)
6. T. Lin, H. Yu, Y. Wang, L. Wang, S.Z. Vatsadze, X. Liu, Z. Huang, S. Ren, M.A. Uddin, B.U. Amin, S. Fahad, J. Mater. Sci. **56**, 18093 (2021)
7. M.T. Ramesan, K. Nushhat, K. Parvathi, T. Anilkumar, J. Mater. Sci. Mater. Electron. **30**, 13719 (2019)
8. C. Taşaltın, T.A. Türkmen, N. Taşaltın, S. Karakuş, J. Mater. Sci. Mater. Electron. **32**, 10750 (2021)
9. M. Vinitha, G. Velraj, J. Mater. Sci. Mater. Electron. **33**, 6627 (2022)
10. T. Das, B. Verma, J. Mater. Sci. Mater. Electron. (2022). https://doi.org/10.1007/s10854-022-08220-x
11. W. Wang, G. Ren, M. Wang, Y. Liu, S. Wu, J. Shen, J. Mater. Sci. Mater. Electron. **29**, 5548 (2018)
12. K. Amruth, K.M. Abhirami, S. Sankar, M.T. Ramesan, Inorg. Chem. Commun. **136**, 109184 (2022)
13. M. Zhang, Z. Yu, H. Yu, Polym. Bull. **77**, 1049 (2020)
14. S. Khademi, B. Pourabbas, K. Foroutani, Polym. Bull. **75**, 4291 (2018)
15. H. Gherras, A. Yahiaoui, A. Hachemaoui, A. Belfedal, A. Dehbi, A. Zeinert, Polym. Polym. Compos. **28**, 265 (2019)
16. J. Simitzis, S. Soulis, D. Triantou, J. Appl. Polym. Sci. **125**, 1928 (2012)
17. Y. Wang, W.B. Ma, L. Guo, X.Z. Song, X.Y. Tao, L.T. Guo, H.L. Fan, Z.S. Liu, Y.B. Zhu, X.Y. Wei, J. Mater. Sci. Mater. Electron. **32**, 6263 (2020)
18. F. Köleli, D. Dündar, J. Appl. Polym. Sci. **109**, 3044 (2008)
19. K. Dhanalakshmi, R. Saraswathi, J. Mater. Sci. **36**, 4107 (2001)
20. M. Mansour Lakourj, R.-S. Norouzian, M. Esfandyar, S. Ghasemir, Mater. Sci. Eng. B **261**, 114673 (2020)
21. P. Jisha, M.S. Suma, M.V. Murugendrappa, S.R. Ananda, J. Mater. Sci. Mater. Electron. **32**, 11243 (2021)
22. M. Radoičić, G.C. Marjanović, Z.V. Šaponjić, M. Mitrić, Z. Konstantinović, M. Stoiljković, J.M. Nedeljković, J. Mater. Sci. **48**, 5776 (2013)
23. K. Yamani, R. Berenguer, A. Benyoucef, E. Morallón, J. Therm. Anal. Calorim. **135**, 2089 (2019)
24. M. Hassanpour, H.S. Hojaghan, M.S. Niasari, A.Y. Faal, J. Mater. Sci. Mater. Electron. **28**, 14678 (2017)
25. K. Parvathi, M.T. Ramesan, Polym. Compos. **43**, 2628 (2022)
26. A.N. Gheymasi, Y. Rajabi, E.N. Zare, Opt. Mater. **102**, 109835 (2020)
27. M. Golshekan, F. Shirini, J. Appl. Polym. Sci. **136**, 48265 (2019)
28. D. Lu, J. Jiang, L. Lu, X. Liao, K.M. Nesterov, R.K. Islamgaliev, R.Z. Valiev, K. Liu, J. Mater. Eng. Perform. **26**, 2110 (2017)
29. S. Sankar, A.A. Naik, T. Anilkumar, M.T. Ramesan, J. Appl. Polym. Sci. **137**, 49145 (2020)
30. M.A. Bekhti, M.S.E. Belardja, M. Lafjah, F. Chouli, A. Benyoucef, Polym. Compos. **42**, 6 (2021)
31. T. Sampreeth, M.A. Al-Maghrabi, B.K. Bahuleyan, M.T. Ramesan, J. Mater. Sci. **53**, 591 (2018)
32. Y. Cheng, C. Lü, Z. Lin, Y. Liu, C. Guan, H. Lü, B. Yang, J. Mater. Chem. **18**, 4062 (2008)
33. A.S. Hassanien, I.M.E. Radaf, A.A. Akl, J. Alloys Compd. **849**, 156718 (2020)
34. S. Sankar, K. Parvathi, M.T. Ramesan, High. Perform. Polym. **32**, 719 (2020)
35. A.V. Jadhav, C.G. Gulgas, A.D. Gudmundsdottir, Eur. Polym. J. **43**, 2594 (2007)
36. S. El-Gamal, M. Elsayed, Polymers **206**, 122911 (2020)
37. S. El-Gamal, A.M. Ismail, R. El-Mallawany, J. Mater. Sci. Mater. Electron. **26**, 7544 (2015)
38. K. Parvathi, B.K. Bahuleyan, M.T. Ramesan, J. Macromol. Sci. A **59**, 466 (2022)
39. M. Elsayed, S. El-Gamal, Phys. Scr. **97**, 055814 (2022)
40. R.D. Balikile, A.S. Roy, S.C. Nagaraju, G. Ramgopal, J. Mater. Sci. Mater. Electron. **28**, 7368 (2017)

41. R. Kandulna, R.B. Choudhary, R. Singh, J. Inorg. Organomet. Polym. **29**, 730 (2019)
42. M. Irfan, A. Shakoor, J. Inorg. Organomet. Polym. Mater. **30**, 1287–1292 (2020)
43. K. Suhailath, B.K. Bahuleyan, M.T. Ramesan, J. Inorg. Organomet. Polym. Mater. **31**, 365 (2021)
44. K. Suhailath, M. Thomas, M.T. Ramesan, Res. Chem. Int. **46**, 2579 (2020)
45. M.H. Najar, K. Majid, M.A. Dar, J. Mater. Sci. Mater. Electron. **28**, 11243 (2017)
46. S. Karoui, H. Chouaib, S. Kamoun, J. Phys. Org. Chem. **33**, e4101 (2020)
47. R. Moučka, N. Kazantseva, I. Sapurina, J. Mater. Sci. **53**, 1995 (2018)
48. N.J.S. Sohi, S. Bhadra, D. Khastgir, Carbon **49**, 1349 (2011)
49. K. Suhailath, M. Thomas, M.T. Ramesan, Polym. Polym. Compos. **29**, 1200 (2021)
50. R.L. McCullough, Compos. Sci. Technol. **22**, 3 (1985)